Sequential magnetic switching in Fe/MgO(001) superlattices

F. Magnus,[1,2,*] T. Warnatz,[1] G. K. Palsson,[1] A. Devishvili,[1,3] V. Ukleev,[1,4,†] J. Palisaitis,[5] P. O. Å. Persson,[5] and B. Hjörvarsson[1]

[1]*Department of Physics and Astronomy, Uppsala University, Box 530, SE-75121 Uppsala, Sweden*
[2]*Science Institute, University of Iceland, Dunhaga 3, IS-107 Reykjavik, Iceland*
[3]*Department of Physical Chemistry, Lund University, Box 124, SE-22100 Lund, Sweden*
[4]*National Research Centre "Kurchatov Institute" B. P. Konstantinov Petersburg Nuclear Physics Institute, 188300 Gatchina, Russia*
[5]*Department of Physics, Chemistry and Biology, Linköping University, SE-58183 Linköping, Sweden*

(Received 16 November 2017; revised manuscript received 7 March 2018; published 24 May 2018)

Polarized neutron reflectometry is used to determine the sequence of magnetic switching in interlayer exchange coupled Fe/MgO(001) superlattices in an applied magnetic field. For 19.6 Å thick MgO layers we obtain a 90° periodic magnetic alignment between adjacent Fe layers at remanence. In an increasing applied field the top layer switches first followed by its second-nearest neighbor. For 16.4 Å MgO layers, a 180° periodic alignment is obtained at remanence and with increasing applied field the layer switching starts from the two outermost layers and proceeds inwards. This sequential tuneable switching opens up the possibility of designing three-dimensional magnetic structures with a predefined discrete switching sequence.

DOI: 10.1103/PhysRevB.97.174424

I. INTRODUCTION

The transition from the current two-dimensional data storage and logic schemes to three-dimensional data structures could significantly improve the performance and capacity of electronic devices. Instead of simply storing and manipulating data in a two-dimensional array of elements, one can envisage stacking data bits on top of each other, thus greatly enhancing the data density [1,2]. One such proposed scheme involves metallic multilayers where adjacent layers are antiferromagnetically coupled through an RKKY-type interlayer exchange coupling. This allows the flipping of magnetic bits to be propagated from layer to layer through the structure as in a shift register [3].

Magnetic tunnel junctions, where two magnetic layers are separated by an insulating barrier, are the cornerstone of many current and proposed spintronic-device concepts such as MRAM [4], magnetic sensors [5], and spin logic devices [6,7]. It has recently been shown that several Fe/MgO/Fe tunnel junctions can be stacked on top of each other in a superlattice (the crystalline counterpart of a multilayer), where the Fe layers are antiferromagnetically coupled through the MgO layers [8]. The interlayer exchange coupling in conjunction with the fourfold magnetocrystalline anisotropy of the epitaxial Fe layers results in a 180° or 90° periodic alignment of adjacent layers at remanence, depending on the MgO layer thickness. A discrete layer-by-layer magnetic switching was also observed, opening up the possibility of creating three-dimensional memory devices or magnetic shift registers. However, the mechanism responsible for the coupling and why it results in a layer-by-layer switching instead of a simultaneous switching of all inner layers of the superlattice is still unclear.

Here we examine the sequence of the discrete magnetic switching in Fe/MgO superlattices using polarized neutron reflectometry. This is the method of choice to determine magnetization depth profiles and can reveal the layer resolved magnetization size and in-plane direction [9]. Knowing the sequence of switching is essential to understand the nature of the interlayer coupling. We show that the switching is sequential, starting from the outermost layers, and confirm that different remanent states can be achieved by changing the MgO thickness.

II. EXPERIMENTAL METHODS

The Fe/MgO superlattices were grown by magnetron sputtering in an ultrahigh vacuum chamber with a base pressure of 2×10^{-9} mbar. The Ar (99.99999% purity) working gas pressure was 2.7×10^{-3} mbar and the substrate temperature during deposition was 165 °C. Fe layers with a constant nominal thickness of 22 Å were deposited from an Fe target (of 99.95% purity) using dc sputtering, whereas the MgO layers were deposited using a MgO target (of 99.9% purity) with a RF source. 10 repetitions of Fe/MgO bilayers were grown, all starting with the growth of Fe on the MgO(001) substrates, ending with a 45 Å thick Pd capping layer. Two MgO thicknesses were studied: 16.4 Å and 19.6 Å.

Polarized neutron reflectometry (PNR) was carried out in the Super ADAM reflectometer at the Institut Laue-Langevin in Grenoble, France [10]. The neutron wavelength was 5.183 Å and polarization and analyzer efficiencies were 99.8% and 99.3% on the incident and receiving ends, respectively. A guide field of 1.5–3.0 mT was used to maintain the neutron polarization parallel to the plane of the films and an electromagnet was used to apply a magnetic field to the sample, in all cases parallel

*fridrikm@hi.is
†Present address: RIKEN Center for Emergent Matter Science (CEMS), Wako 351-0198, Japan.

to the guide field. The data reduction package SARED was used for data analysis. The data was normalized by a monitor to account for fluctuations in the neutron flux and to correct for points measured for different lengths of time. A constant slit opening for the entire data set was chosen such that the sample was constantly overilluminated and this was included as a fitting parameter in the fitting procedure. Complementary x-ray reflectivity (XRR) measurements were performed in a Philips X-Pert Pro MRD diffractometer (Cu $K_\alpha = 1.5418$ Å) on the same samples and finally the PNR and XRR data was fitted together using the GenX fitting program [11].

The local crystal structure and layering was investigated by scanning transmission electron microscopy (STEM) combined with high angle annular dark field imaging in the double-corrected Linköping FEI Titan^3 60–300, operated at 300 kV. STEM images were recorded under strong elemental contrast conditions using an optimized 30 mrad convergence semiangle which provided sub-Ångström resolution probes with 0.1 nA current. The TEM samples were prepared using a traditional "sandwich" method which included sample cutting, mounting into the support grid, glueing, and mechanical polishing. Electron transparency of the sample was achieved by Ar^+ ion milling with 5 keV ion energy where the ion energy was gradually reduced to 2 keV during the final step of milling to minimize the surface damage.

Magnetization measurements were performed at room temperature using a magneto-optical Kerr effect (MOKE) setup, in a longitudinal geometry, using p-polarized light as well as with a vibrating sample magnetometer (VSM). A magnetic field was applied in the plane of the films and the magnetic response measured parallel to the applied field.

III. RESULTS

Representative cross-sectional STEM images of one of the samples can be seen in Fig. 1, illustrating the structural quality of the superlattices. The low magnification image [Fig. 1(a)] shows an entire stack with 10 repetitions of Fe/MgO bilayers. The layers are continuous and flat with sharp interfaces throughout the 300 nm lateral range shown. The epitaxial nature of the layers can be seen in the high resolution image [Fig. 1(b)] where the Fe(001) and MgO(001) are clearly in registry with each other. This epitaxial relationship is maintained throughout the stack and is obtained upon a 45° in-plane rotation of the Fe lattice with respect to the MgO lattice. PNR measurements of the Fe (21.3 Å)/MgO (19.6 Å) superlattice (the "thick-MgO" sample) and the Fe (22.0 Å)/MgO (16.4 Å) superlattice (the "thin-MgO" sample) in a saturated (collinear) magnetic state are shown in Fig. 1(c). The magnetization of the Fe layers was saturated by applying a magnetic field of 570 mT along the easy axis (the saturation field along the hard axis is approximately 100 mT). Well defined multilayer (superlattice) peaks are observed, whose position corresponds to the Fe/MgO bilayer thickness, as well as clear total thickness Kiessig fringes. Fitting of the reflectivity curves, together with XRR data from the same samples, gives the thickness values for Fe and MgO layers quoted above and their top-interface root mean square roughnesses are 2.4 Å and 2.0 Å, respectively, in the thick-MgO sample and 2.2 Å and 1.8 Å in the thin-MgO

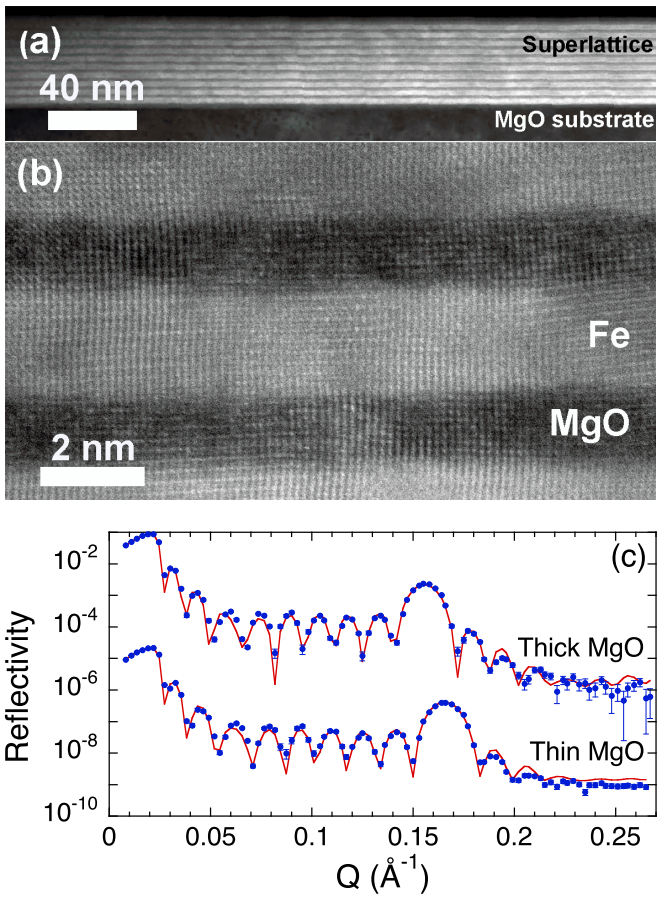

FIG. 1. Structure of the superlattices. (a) Cross sectional STEM image of a sample with 10 repetitions of Fe/MgO bilayers showing the entire sample thickness. (b) Atomic resolution STEM image showing the well-defined ordering of the Fe(001) and MgO(001) lattice. (c) PNR measurements (non-spin-flip channel) of an Fe (21.3 Å)/MgO (19.6 Å) superlattice (the thick-MgO sample) and an Fe (22.0 Å)/MgO (16.4 Å) superlattice (the thin-MgO sample), both with 10 repetitions, in a saturated (collinear) magnetic state. The thin-MgO data are shifted by a factor of 10^{-3} for clarity.

sample. The layer densities were allowed to vary by ±5% from the literature values of 7.87 g/cm^3 for Fe and 3.58 g/cm^3 for MgO. The magnetic moment of the Fe was determined by VSM measurements as $2.35 \pm 0.10\ \mu_B$/atom and was not fitted. A more detailed account of the structural properties of the samples can be found in Ref. [8].

The discrete magnetization switching of the Fe layers in the thick-MgO sample can be seen in the MOKE measurements presented in Fig. 2(a). The magnetization reversal takes place through a series of steps (eleven in total) and when the field is reduced from saturation the magnetization reversal starts well before the field is inverted, indicating an antiferromagnetic interlayer exchange coupling between the Fe layers. Such an antiferromagnetic interlayer exchange coupling has been seen previously in single Fe/MgO/Fe tunnel junctions in a number of studies [12–16]. VSM measurements (which give the volume averaged total magnetic moment) confirm that the first step when increasing the field from remanence corresponds to one tenth of the saturation moment, or exactly one Fe layer. The

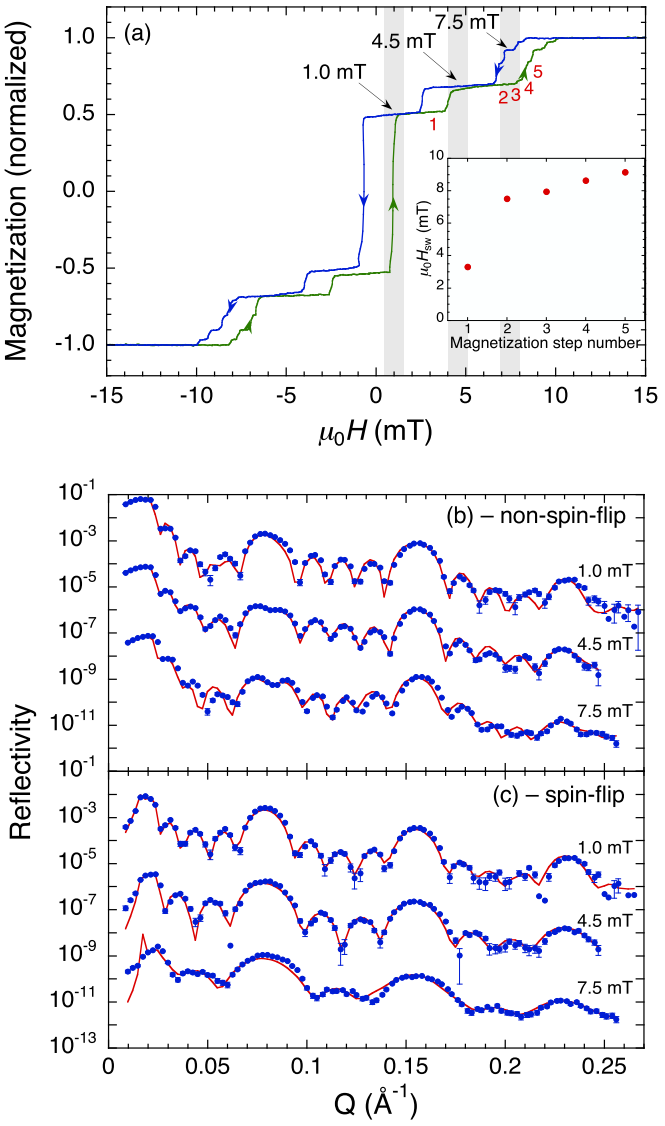

FIG. 2. (a) Room-temperature in-plane magnetization curves of the thick-MgO sample. The magnetic field was applied parallel to the Fe in-plane easy axis (the Fe[100] direction). The down field sweep is blue and the up field sweep is green. The field values at which the PNR measurements were performed are indicated. Inset: The switching field for each magnetization step, labeled with red numbers in the main panel. (b) and (c) PNR measurements on the same sample in the three different applied fields. The data at 4.5 and 7.5 mT are shifted by a factor of 10^{-3} and 10^{-6}, respectively, for clarity. Both the non-spin-flip (b) and spin-flip (c) channels are shown. The data are shown by blue dots whereas the red curves are fits.

discrete magnetization switching in steps corresponding to the magnetic moment of a single layer suggests a layer-by-layer magnetic switching, most likely via 90° domain wall nucleation and motion within each layer. In addition, the remanent moment is half the saturation moment, indicating that every other layer points along the sensitivity axis of the measurement and the others are perpendicular to this axis. This is consistent with an interplay between the strong fourfold magnetocrystalline anisotropy of the Fe layers and an antiferromagnetic interlayer exchange coupling [8], although we cannot rule out the presence of a biquadratic coupling term as well [16].

The inset shows the switching fields H_{sw} corresponding to each step in the magnetization. The switching energy and therefore the coupling strength experienced by each layer is proportional to the switching field for that layer. The final magnetization step is representative of the maximum interlayer exchange coupling and is approximately one-tenth the size of the magnetocrystalline anisotropy (determined from comparing H_{sw} and the saturation field of a hard-axis magnetization measurement [see Ref. [8]]). The first step corresponds to a coupling which is only approximately one third of the strongest coupling. We will come back to this point in the Discussion section. The size of the coupling is similar to that found in other studies but in our case it extends through MgO layers which are significantly thicker [8]. The reasons for this are as yet unknown but it has been shown that the size and sign of the coupling is strongly affected by a number of factors such as strain [17], impurities/vacancies in the MgO [13,14,17], and interface roughness [18]. These factors are highly sensitive to the growth conditions which vary somewhat between experiments. Furthermore, other studies have been performed on single MgO layers and not superlattices. It is worth noting that interface roughness can also lead to interlayer coupling of a magnetostatic origin, which can be either ferromagnetic (for correlated roughness [19]) or antiferromagnetic (for uncorrelated roughness [20]). However, we expect this effect to be weak in our samples since the roughness is small and the coupling decreases with increasing roughness.

In order to establish the sequence of magnetic switching, PNR measurements have been performed [Figs. 2(b) and 2(c)] at different applied field values corresponding to the remanent state (1.0 mT), the first plateau when increasing the field from remanence (4.5 mT), and centered at the third plateau (7.5 mT), as indicated in Fig. 2(a). We estimate that the uncertainty in the applied field during PNR measurements relative to the applied field in the MOKE measurements is ±0.5 mT as indicated by the gray shaded areas in the figure. Therefore, we cannot say whether the measurement at 7.5 mT corresponds to the second, third, or fourth plateau. In all cases the sample was first saturated along the positive field direction before reducing the field to the values shown. The PNR data for the non-spin-flip channel (R^{++}) and one of the two spin-flip channels (R^{-+}) are shown in Figs. 2(b) and 2(c), respectively.

The non-spin-flip measurement at remanence (1.0 mT) shows a Bragg peak at a scattering vector value $Q = 2\pi/\Lambda = 0.155$ Å^{-1} where Λ is the Fe/MgO bilayer thickness. This peak is due to the structural periodicity of the superlattice. In addition, there is a Bragg peak at half of this Q value which corresponds to twice the structural periodicity. The non-spin-flip channel is sensitive to the magnetization along the polarization direction of the neutrons [9] which is the same as the applied field direction. This Q-half peak is therefore purely magnetic in origin and shows that the magnetization along the neutron polarization axis has twice the period of the superlattice, i.e., that every other Fe layer points along this direction. As the field is increased the Q-half peak broadens indicating that fewer layers are arranged in this periodic arrangement, meaning that more and more layers are aligning

TABLE I. Magnetization angles of the Fe layers in the thick-MgO sample, as determined from fitting the PNR data taken at the field values 1.0 mT (remanence), 4.5 mT (1st plateau), and 7.5 mT (2nd plateau). 0° is parallel to the applied field direction. The angles corresponding to a layer switching have been highlighted in bold in the first and second step. Typical uncertainties are between ±5° and ±10°, based on allowing a 5% variation in the figure of merit.

Fe layer	Remanence	1st plateau	2nd plateau
1	89°	**0°**	**4°**
2	10°	−4°	3°
3	90°	87°	**9°**
4	15°	10°	−12°
5	91°	84°	99°
6	−12°	0°	−15°
7	78°	87°	81°
8	−7°	-8°	25°
9	76°	85°	88°
10	−2°	9°	9°

with the applied field. At saturation the Q-half peak disappears entirely [see Fig. 1(c)] as the magnetic periodicity becomes identical to the structural periodicity.

The spin-flip signal on the other hand is entirely due to magnetic scattering and is sensitive to the magnetization component which is perpendicular to the neutron polarization axis [9]. In the remanent state we again see a Bragg peak corresponding to twice the periodicity of the superlattice (as well as higher order peaks) showing that every other Fe layer has a magnetization which is perpendicular to the neutron polarization. With increasing field these Bragg peaks remain but are broadened, again indicating that fewer layers are arranged in this arrangement with twice the structural periodicity. In addition, we see clear Kiessig fringes in between the Bragg peaks which arise from the total thickness (extent in the out-of-plane direction) of the periodic arrangement of magnetic moments. With increasing applied field the spacing of the Kiessig fringes increases (the number of fringes appears to decrease) which means that the extent of the periodic arrangement of moments is decreasing. Again this tells us that layers are increasingly aligning with the applied field, starting from the outermost layers and moving inward.

In order to establish this quantitatively we have fitted the PNR curves using the GenX fitting software. The structural parameters, determined by fitting the PNR saturation curves and XRR, were fixed and the PNR curves at other fields fitted by allowing only the direction of magnetization of each Fe layer to vary. Since the films have a strong fourfold magnetocrystalline anisotropy (significantly larger than the interlayer exchange coupling [8]) we perform the fitting in two steps, where we first allow only magnetization angles along the easy axes (i.e., 0°, 90°, etc., with 0° being the applied field direction), and then use that result as a starting condition for an unconstrained fit of the magnetization direction. The results of the fitting are shown in Figs. 2(b) and 2(c). The resulting magnetization angles are shown in Table I. The magnetization vectors are shown schematically in Fig. 3. We find that the remanent state is one where adjacent layers point at 90° to one another, with

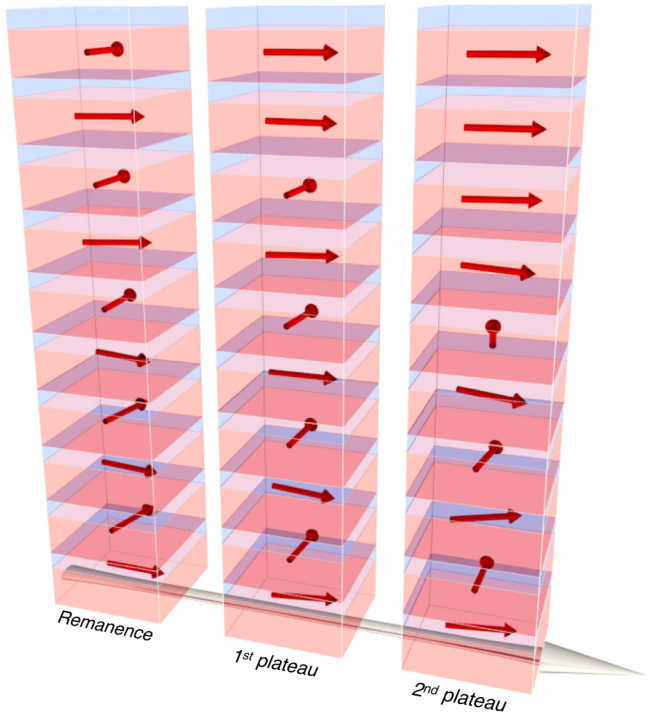

FIG. 3. An illustration of the thick-MgO superlattice with magnetization vectors determined from the PNR measurement (Table I). MgO layers are blue and Fe layers red but the thickness of the layers is not to scale. Layer one is the top layer. The gray arrow shows the direction of the applied field, which increases from left to right.

every other layer pointing along the direction of saturation and every other layer perpendicular to this direction. Note that the perpendicular layers could point along either the positive or negative transverse direction. At the first plateau the outermost layer has flipped from the transverse direction to the applied field direction. This can be understood from the fact that the outermost layers experience only half the interlayer exchange coupling of the other layers since they only have one nearest neighbor Fe layer. At the second-fourth plateau the third outermost layer has flipped (the second outermost layer which was pointing along the transverse direction at remanence), showing that this is in fact the second plateau.

Figure 4(a) shows the magnetization curve for an Fe (22.0 Å)/MgO (16.4 Å) superlattice with 10 repetitions (the "thin-MgO" sample). A series of steps is also observed but in between the magnetization varies approximately linearly. Again, the magnetic reversal starts well before the field is inverted but here the remanent magnetization is zero. This indicates a fully antiferromagnetic alignment of layers at zero applied field which is due to the exponentially increasing antiferromagnetic interlayer exchange coupling with decreasing MgO layer thickness [8,12].

The PNR results at remanence (3 mT) and at 47 mT (corresponding to the third from last plateau) are shown in Figs. 4(b) and 4(c), respectively. Again, the Bragg peak at $Q = 0.165$ Å^{-1} in the non-spin-flip channel is due to the structural periodicity of the superlattice. No such peak is present in the spin-flip channel meaning that no such periodicity

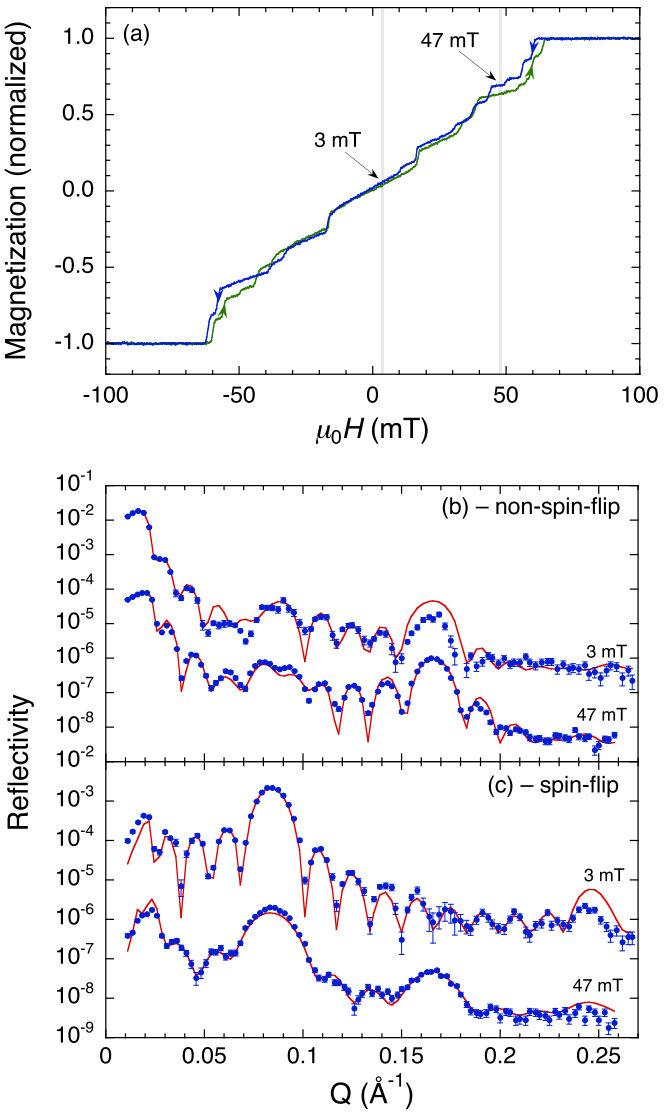

FIG. 4. (a) Room-temperature in-plane magnetization curves of the thin-MgO sample. The magnetic field was applied parallel to the Fe in-plane easy axis (the Fe[100] direction). The down field sweep is blue and the up field sweep is green. The field values at which the PNR measurements were performed are indicated. (b) and (c) PNR measurements on the same sample in the two different applied fields. The data at 47 mT are shifted by a factor of 10^{-3} for clarity. Both the non-spin-flip (b) and spin-flip (c) channels are shown. The data are shown by blue dots whereas the red curves are fits.

exists in the magnetic moment in the transverse direction. The spin-flip channel on the other hand shows a Q-half peak corresponding to a magnetic alignment in the transverse direction with twice the structural period. The broadening of the Bragg peaks and the larger spacing of Kiessig fringes at 47 mT shows that the extent of the periodic magnetic alignment in the transverse direction is decreasing with increasing field.

Table II shows the magnetization angles of each layer as determined by fitting the PNR curves. In the thin-MgO case the interlayer exchange coupling and magnetocrystalline anisotropy are comparable in size and therefore we do not impose any restriction on the magnetization angles. The magnetization vectors are shown schematically in Fig. 5. At remanence all layers are pointing along the transverse direction (perpendicular to the applied field) with almost 180° between adjacent layers. This configuration is expected for antiferromagnetically coupled superlattices which undergo a spin-flop transition in a small applied field [21,22]. When the field is increased the moments start to rotate towards the field direction, in stark contrast to the abrupt switching in the thick-MgO sample. Without magnetic anisotropy, the moments would rotate coherently resulting in a linear hysteresis curve [22]. However, here we have a strong magnetocrystalline anisotropy which makes +45° and −45° highly energetically unfavorable directions resulting in the small jumps in the otherwise linearly increasing magnetization. The magnetic angles found by PNR at 47 mT show that this switching does not occur uniformly throughout the thickness of the superlattice but sequentially, starting from both the top and bottom layers. Note that this is different from the thick-MgO case, where one of the outermost layers already points along the field direction at remanence. A large spread in angles is also seen and layer three even appears to be pointing along a hard axis. This is due to the large interlayer coupling relative to the anisotropy but could also be partly a result of domain structure where an average magnetization angle is obtained from scattering from both flipped and nonflipped domains [23].

TABLE II. Magnetization angles of the Fe layers in the thin-MgO sample, as determined from fitting the PNR data taken at the field values 3.0 mT (remanence) and 47 mT (3rd from last plateau). The angles were unconstrained, with 0° parallel to the applied field direction. The angles corresponding to a layer switching have been highlighted in bold. The uncertainty in the fitting values (determined from a 5% variation in the figure of merit) is approximately ±10°.

Fe layer	Remanence	3rd last plateau
1	−78°	**−29°**
2	89°	**7°**
3	−77°	**−46°**
4	84°	**13°**
5	−72°	−86°
6	90°	**17°**
7	−67°	−81°
8	92°	**18°**
9	−73°	**6°**
10	87°	**−6°**

IV. DISCUSSION

The fitting shows that the switching starts at the outermost layer(s) and works its way inwards. To test the robustness of this result we have carried out simulations with different switching sequences for each plateau of the thick-MgO sample (Fig. 2) and compared them qualitatively. The simulated curves for the non-spin-flip channel (up-up) are shown in Figs. 6(a) and 6(b), corresponding to the first and second plateaux, respectively. For the first plateau, we compare three different cases: switching at the top of the superlattice, switching at the bottom, and switching a middle layer. The magnetization

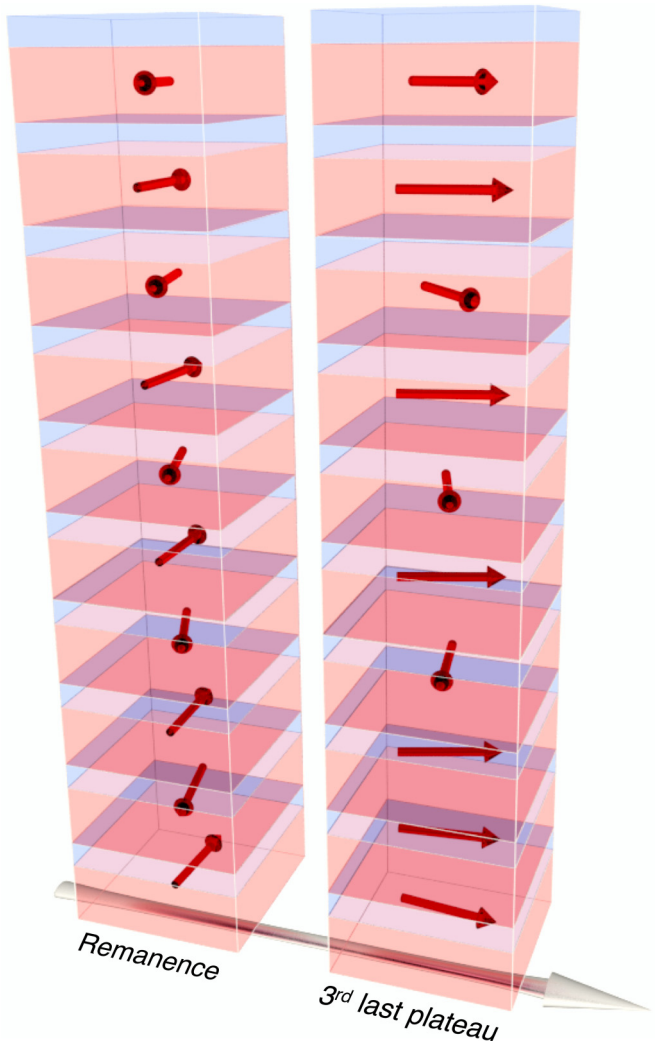

FIG. 5. An illustration of the thin-MgO superlattice with magnetization vectors determined from the PNR measurement (Table II). MgO layers are blue and Fe layers red but the thickness of the layers is not to scale. Layer one is the top layer. The gray arrow shows the direction of the applied field, which increases from left to right.

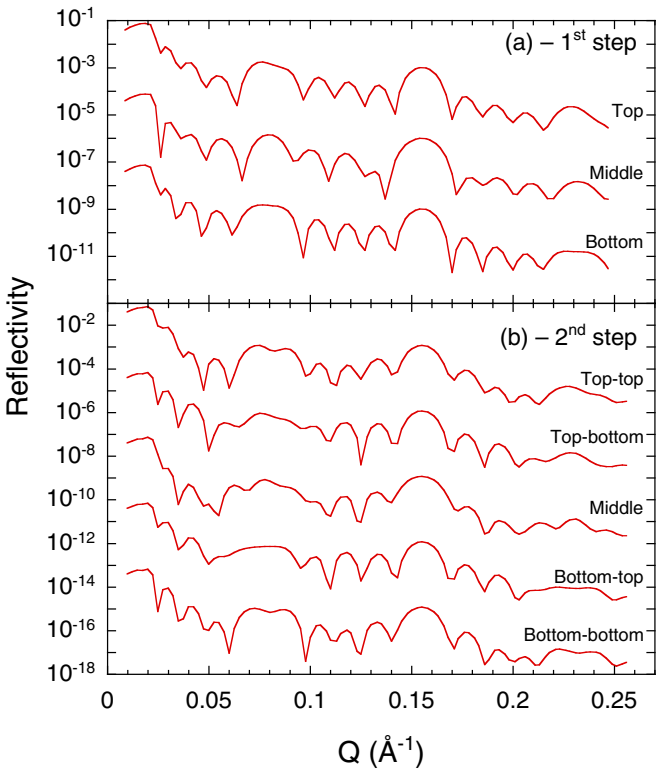

FIG. 6. Simulations of the PNR up-up polarization channel for different switching sequences. (a) Comparison of switching one top layer, one bottom layer, or one middle layer in the first magnetization step. (b) Comparison of switching two next-nearest neighbor top layers (top-top), a top and a bottom layer (top-bottom), two middle layers (middle), a bottom and a top layer (bottom-top), and two next-nearest neighbor bottom layers (bottom-bottom). The curves are shifted for ease of comparison. The magnetization angles are shown explicitly in Tables III and IV.

angles are shown in Table III. There are clear differences between these three scenarios, particularly evident in the width and shape of the first Bragg peak but also in the structure of the Kiessig fringes. Only switching at the top is consistent with our data and this is qualitatively the same as the result which is presented in Fig. 2. The same result is also obtained for the spin-flip channels (not shown). We can therefore state with confidence that the switching starts from the outermost layers and not the center and from which end it starts. For the second plateau we have compared flipping two second nearest neighbor layers from the top (similar to the result in Table I) or bottom of the stack to flipping one layer at each end or flipping two central layers. The magnetization angles for these different cases are shown in Table IV. Flipping one layer at each end or flipping two central layers results in curve shapes which are markedly different from the ones observed, again borne out by the shape and width of the first Bragg peak. Therefore we can be certain that the flipping is sequential from one end in the thick-MgO case.

The observed sequence of switching is hard to rationalize in terms of only nearest neighbor interlayer exchange interactions. It is clear that to first approximation the outermost

TABLE III. Magnetization angles of the Fe layers for the simulations of different switching sequences, corresponding to the first magnetization step. The associated reflectivity curves are shown in Fig. 6(a).

Fe layer	Top	Bottom	Middle
1	0°	0°	0°
2	0°	90°	90°
3	90°	0°	0°
4	0°	90°	90°
5	90°	0°	0°
6	0°	90°	0°
7	90°	0°	0°
8	0°	90°	90°
9	90°	0°	0°
10	0°	0°	90°

TABLE IV. Magnetization angles of the Fe layers for the simulations of different switching sequences, corresponding to the second magnetization step. The associated reflectivity curves are shown in Fig. 6(b).

Fe layer	Top-top	Top-bottom	Middle	Bottom-top	Bottom-bottom
1	0°	0°	90°	0°	0°
2	0°	0°	0°	0°	90°
3	0°	90°	0°	0°	0°
4	0°	0°	0°	90°	90°
5	90°	90°	0°	0°	0°
6	0°	0°	0°	90°	90°
7	90°	90°	90°	0°	0°
8	0°	0°	0°	90°	0°
9	90°	0°	90°	0°	0°
10	0°	0°	0°	0°	0°

layers experience only half the interlayer exchange coupling of the inner layers. Assuming only nearest neighbor interactions, all the inner layers should be equivalent and should switch simultaneously. Our data shows that this is not the case. In fact, the inset of Fig. 2(a) shows that the coupling strength being overcome at the first magnetization step is only a third of the coupling strength of the innermost layer and that the coupling strength increases for each layer towards the middle of the superlattice. The assumption of only nearest-neighbor interactions cannot explain such a coupling strength dependence. However, the thick-MgO results could be justified by the presence of a second-nearest neighbor ferromagnetic interaction, which would favor the switching of the third topmost layer in the second step and then the layers below in sequence. Similarly, the thin-MgO results are consistent with a beyond-nearest neighbor antiferromagnetic interaction since this would result in the middle layers being most strongly antiferromagnetically coupled and switching at the highest field.

In order to test the significance of beyond-nearest neighbor interlayer exchange coupling we have carried out modeling of the layer magnetizations by minimization of the total areal energy density of the system. This approach is only useful in the thin-MgO case, since the dynamics of the switching are not taken into account and thus metastable magnetic states can not be expected to be found reliably. Therefore we restrict ourselves to the high interlayer exchange coupling regime. The phenomenological expression for the areal energy density of layer i of the superlattice is

$$E_i = -\tfrac{1}{2}J_1[\cos(\phi_{i-1}-\phi_i)+\cos(\phi_i-\phi_{i+1})] + K d_{\mathrm{Fe}}\sin^2\phi_i\cos^2\phi_i - \mu_0 H M_s d_{\mathrm{Fe}}\cos(\phi_i-\phi_H), \quad (1)$$

where J_1 is the bilinear interlayer exchange coupling strength (antiferromagnetic for $J_1 < 0$), K is the magnetocrystalline anisotropy constant, d_{Fe} is the Fe layer thickness, M_s is the saturation magnetization, and H is the applied field, at an angle ϕ_H. The sum of the energy for all layers is minimized with respect to the magnetization angle of each layer ϕ_i, for different applied field values. For the outermost layers, only one of the two interlayer exchange coupling terms is present. The results for Eq. (1), using $J_1 = -1.0\times10^{-4}$ J/m^2 and $K = 5.0\times10^4$ J/m^3 are shown in Fig. 7. The model reproduces the main observed features very well. At small applied field the spin-flop transition gives an antiferromagnetic, perpendicular spin arrangement. As the field increases the spins rotate coherently towards the applied field direction and the outermost layers flip parallel to the field. Eventually the magnetization is saturated along the field direction. To model next-nearest neighbor (NNN) interlayer coupling we add an energy term to Eq. (1),

$$E_i^{\mathrm{NNN}} = -\tfrac{1}{2}J_2[\cos(\phi_{i-2}-\phi_i)+\cos(\phi_i-\phi_{i+2})] \quad (2)$$

with a NNN interlayer exchange coupling strength J_2. Here, only one of the two terms applies for the two outermost layers at each end of the superlattice. The results, with $J_2 = -1.0\times10^{-5}$ J/m^2 and J_1 and K the same as before, are shown in Fig. 8 at the same field values as in the nearest neighbor case. Some clear differences are observed at the higher field values. At 52.5 mT the second outermost layer at the bottom has flipped and at 60 mT the second outermost layer at the top has also flipped. This is a direct result of the next-nearest neighbor antiferromagnetic interlayer exchange coupling and its truncation at the ends of the superlattice. The field required to saturate the magnetization is also increased somewhat due to the higher overall antiferromagnetic coupling (not shown). This is in good qualitative agreement with the PNR results for the thin-MgO sample. It is also worth pointing out that in both the nearest and next-nearest neighbor case we see an almost 90° alignment of adjacent layers, reminiscent of the thick-MgO samples, although a nonzero field is required to stabilize this state in the purely magnetostatic picture.

Beyond-nearest neighbor interlayer exchange interactions have been predicted theoretically for metallic spacers where a non-negligible oscillatory coupling between next-nearest neighbor magnetic layers was calculated [24]. This was demonstrated experimentally in a magnetic semiconductor multilayer, where next-nearest neighbor interlayer exchange coupling was invoked to explain a sequential switching of the magnetic layers [25]. Furthermore, it has been shown in Fe/V superlattices that the dependence of the ordering temperature on number of bilayer repeats is not consistent with only nearest neighbor interactions [26]. Although the interaction mechanism is different in a metallic superlattice, similar arguments could apply in the Fe/MgO case. In addition, it is known that the interaction can be either ferromagnetic or antiferromagnetic in the Fe/MgO system, depending on the thickness of the layers, strain, and other factors [17] and recently, a metalliclike oscillatory interaction has even been found in very thin MgO layers [18]. Therefore it is not inconceivable that longer-range interactions could have a different sign to the nearest neighbor interaction.

V. CONCLUSIONS

Polarized neutron reflectivity measurements have been carried out on Fe/MgO superlattices, where the Fe layers are coupled through the MgO by an antiferromagnetic interlayer exchange coupling, in order to determine the exact sequence of magnetization switching. We have found that when increasing

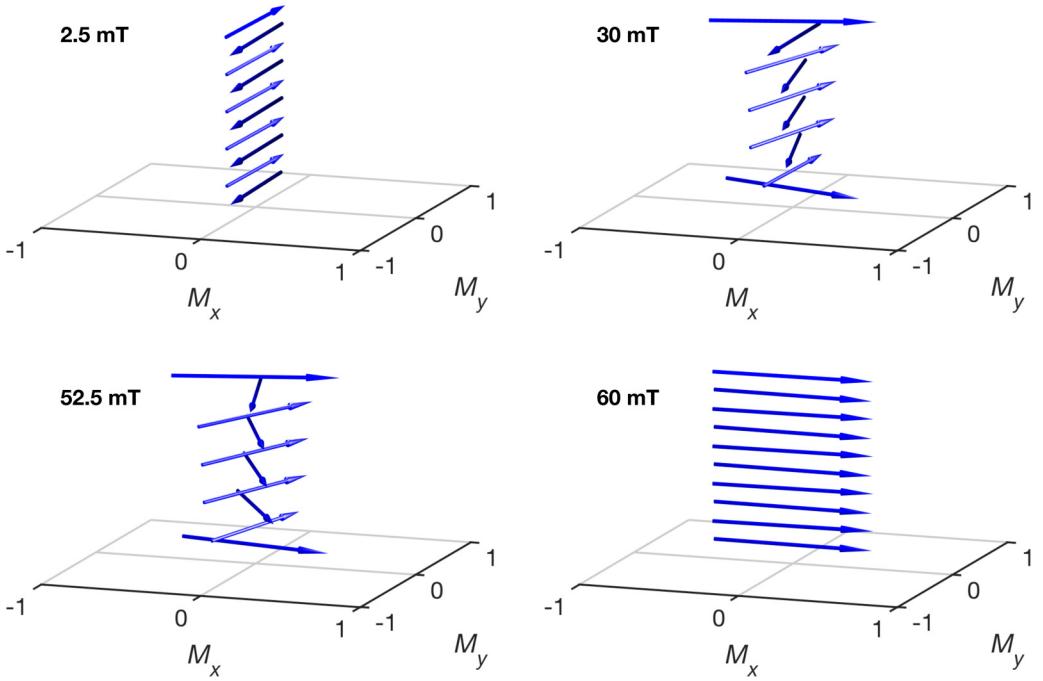

FIG. 7. Modeling of the magnetization of the superlattice, based on minimization of the total areal energy density, assuming only nearest neighbor antiferromagnetic interlayer exchange interactions. The field is applied along the x axis and four different field values are shown, as labeled in the figure. The longitudinal and transverse magnetization is normalized.

the applied field from zero the outermost Fe layer switches first followed by its next nearest neighbor, in the case of thick MgO layers where the interlayer exchange coupling is smaller than the anisotropy. In thin MgO layers, which are dominated by the antiferromagnetic interlayer exchange coupling, both outermost layers switch first followed by their nearest neighbors. Such a sequential switching can be rationalized by assuming interactions beyond nearest neighbor layers. With

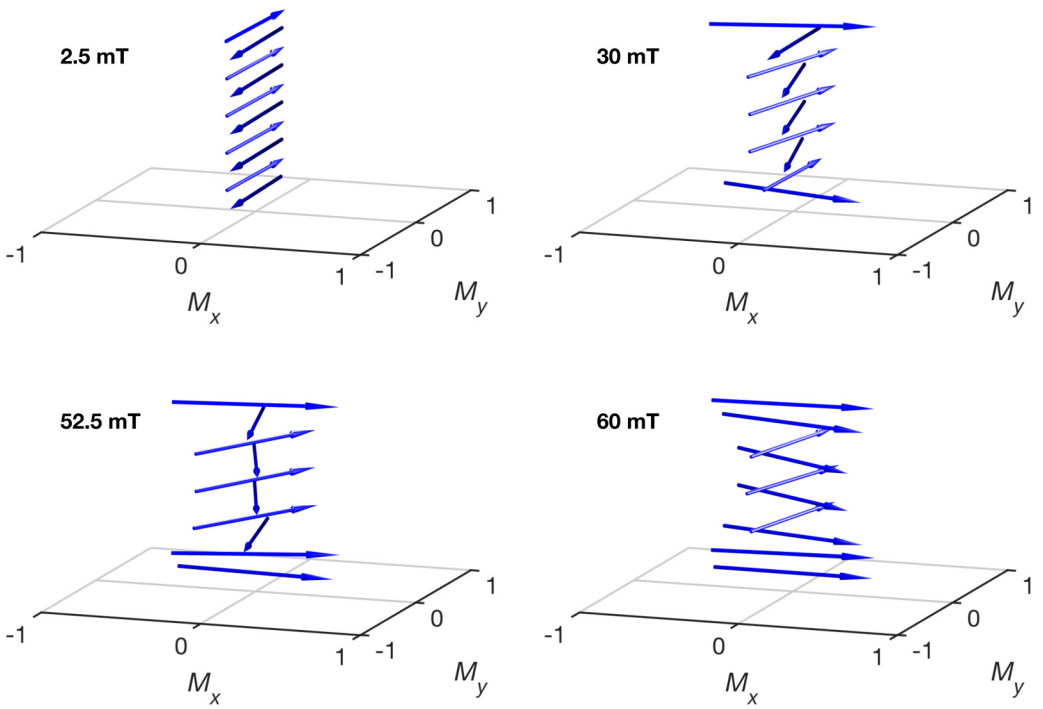

FIG. 8. Modeling of the magnetization of the superlattice, as in Fig. 7, but taking into account both nearest neighbor and next-nearest neighbor antiferromagnetic interlayer exchange interaction parameters. The field is applied along the x axis and four different field values are shown, as labeled in the figure. The longitudinal and transverse magnetization is normalized.

the sequence of magnetic switching established, it is possible to start designing structures with specific switching properties. This could for example be achieved by varying the thickness of individual MgO layers to change the interlayer exchange coupling on a layer-by-layer basis or by varying the thickness of the Fe layers to change the anisotropy. This possibility of having controllable, discrete, and sequential switching in an Fe/MgO-based stacked magnetic tunnel junction structure is interesting for future three-dimensional magnetic storage devices.

ACKNOWLEDGMENTS

This work was funded by the Swedish research council (VR) and the Knut and Alice Wallenberg foundation (KAW). In particular, KAW is acknowledged for their support of the Linköping electron microscopy laboratory. P.O.Å.P. acknowledges funding from the Swedish Foundation for Strategic Research (SSF) through the Research Infrastructure Fellow Program (RIF-0074). The authors thank Prof. Bengt Lindgren for useful discussions.

[1] S. S. P. Parkin, M. Hayashi, and L. Thomas, Science **320**, 190 (2008).
[2] S. Parkin and S. H. Yang, Nat. Nanotech. **10**, 195 (2015).
[3] R. Lavrijsen, J.-H. Lee, A. Fernández-Pacheco, D. C. M. C. Petit, R. Mansell, and R. P. Cowburn, Nature (London) **493**, 647 (2013).
[4] W. J. Gallagher and S. Parkin, IBM J. Res. Dev. **50**, 5 (2006).
[5] P. P. Freitas, R. Ferreira, S. Cardoso, and F. Cardoso, J. Phys.: Condens. Matter **19**, 165221 (2007).
[6] R. Jansen, Nat. Mater. **11**, 400 (2012).
[7] A. Brataas, A. D. Kent, and H. Ohno, Nat. Mater. **11**, 372 (2012).
[8] R. Moubah, F. Magnus, T. Warnatz, G. K. Palsson, V. Kapaklis, V. Ukleev, A. Devishvili, J. Palisaitis, P. O. A. Persson, and B. Hjörvarsson, Phys. Rev. Appl. **5**, 044011 (2016).
[9] H. Zabel, Appl. Phys. A **58**, 159 (1994).
[10] A. Vorobiev, A. Devishvilli, G. Pálsson, H. Rundlöf, N. Johansson, A. Olsson, A. Dennison, M. Wollf, B. Giroud, O. Aguettaz, and B. Hjörvarsson, Neutron News **26**, 25 (2015).
[11] M. Björck and G. Andersson, J. Appl. Crystallogr. **40**, 1174 (2007).
[12] J. Faure-Vincent, C. Tiusan, C. Bellouard, E. Popova, M. Hehn, F. Montaigne, and A. Schuhl, Phys. Rev. Lett. **89**, 107206 (2002).
[13] M. Y. Zhuravlev, E. Y. Tsymbal, and A. V. Vedyayev, Phys. Rev. Lett. **94**, 026806 (2005).
[14] T. Katayama, S. Yuasa, J. Velev, M. Y. Zhuravlev, S. S. Jaswal, and E. Y. Tsymbal, Appl. Phys. Lett. **89**, 112503 (2006).
[15] C. Bellouard, J. Faure-Vincent, C. Tiusan, F. Montaigne, M. Hehn, V. Leiner, H. Fritzsche, and M. Gierlings, Phys. Rev. B **78**, 134429 (2008).
[16] Y. F. Chiang, J. J. I. Wong, X. Tan, Y. Li, K. Pi, W. H. Wang, H. W. K. Tom, and R. K. Kawakami, Phys. Rev. B **79**, 184410 (2009).
[17] H. X. Yang, M. Chshiev, A. Kalitsov, A. Schuhl, and W. H. Butler, Appl. Phys. Lett. **96**, 262509 (2010).
[18] C. Bellouard, A. Duluard, E. Snoeck, Y. Lu, B. Negulescu, D. Lacour, C. Senet, S. Robert, N. Maloufi, S. Andrieu, M. Hehn, and C. Tiusan, Phys. Rev. B **96**, 134416 (2017).
[19] L. Néel, C. R. Acad. Sci. **255**, 1676 (1962).
[20] S. Demokritov, E. Tsymbal, P. Grunberg, W. Zinn, and I. K. Schuller, Phys. Rev. B **49**, 720 (1994).
[21] S. S. P. Parkin, A. Mansour, and G. P. Felcher, Appl. Phys. Lett. **58**, 1473 (1991).
[22] P. Poulopoulos, P. Isberg, W. Platow, W. Wisny, M. Farle, B. Hjörvarsson, and K. Baberschke, J. Magn. Magn. Mater. **170**, 57 (1997).
[23] B. P. Toperverg, Phys. Met. Metallogr. **116**, 1337 (2015).
[24] J.-H. Han and H.-W. Lee, Phys. Rev. B **86**, 174426 (2012).
[25] S. Chung, S. Lee, T. Yoo, H. Lee, J.-H. Chung, M. S. Choi, S. Lee, X. Liu, J. K. Furdyna, J.-H. Han, H.-W. Lee, and K.-J. Lee, New J. Phys. **15**, 123025 (2013).
[26] M. Ahlberg, M. Marcellini, A. Taroni, G. Andersson, M. Wolff, and B. Hjörvarsson, Phys. Rev. B **81**, 214429 (2010).